Supporting Information for

"New Insights Into the Short-Range Structures of Microporous Titanosilicates as Revealed by $^{47/49}$Ti, ^{23}Na, ^{39}K, and ^{29}Si Solid-State NMR Spectroscopy"

Jun Xu,[a] Bryan Lucier,[a] Zhi Lin,[b] Andre Sutrisno,[a] Victor V. Terskikh,[c] and Yining Huang[a,*]

[a] Department of Chemistry, *The* University of Western Ontario, London, Ontario, Canada N6A 5B7

[b] Department of Chemistry, CICECO, University of Aveiro, 3810 Aveiro, Portugal

[c] Department of Chemistry, University of Ottawa, Ottawa, Ontario, Canada, K1N 6N5

*Corresponding author, Tel: (519)661-2111 x 86384, Email: yhuang@uwo.ca.

Table of Contents

Item	Page
Figure S1. Powder XRD patterns	S2
Table S1. $^{47/49}$Ti SSNMR acquisition parameters	S3
Figure S2. $^{47/49}$Ti SSNMR echo spectra of natisite, AM-1, and AM-4	S4
Section S1. ^{29}Si and ^{23}Na SSNMR experimental parameters	S5
Table S2. ^{23}Na SSNMR acquisition parameters	S6
Section S2. ^{23}Na MAS and 3QMAS spectra	S6
Figure S3. ^{23}Na MAS SSNMR spectra at 9.4 T	S6
Figure S4. ^{23}Na 3QMAS spectra at 9.4 T	S8
Section S3. ^{29}Si MAS SSNMR spectra	S9
Figure S5. ^{29}Si MAS SSNMR spectra at 9.4 T	S9
Figure S6. Two Polymorphs of ETS-10	S10
Section S4. $^{47/49}$Ti and ^{23}Na SSNMR experiments on ETS-4	S11
Figure S7. Structure and $^{47/49}$Ti static spectra of ETS-4 at 21.1 T	S13
• ***Appendix A:*** *Plane-wave DFT calculations of ^{23}Na, ^{29}Si, and $^{47/49}$Ti NMR tensor parameters*	S14
Table A1. Experimental and calculated ^{29}Si NMR parameters	S16
Table A2. Experimental and calculated ^{23}Na NMR parameters	S17
Table A3. Experimental and calculated ^{49}Ti NMR parameters	S18
Figure A1. Correlation of experimental and calculated NMR parameters	S19
Figure A2. Correlation of ^{23}Na chemical shifts versus shieldings	S20
References	S20

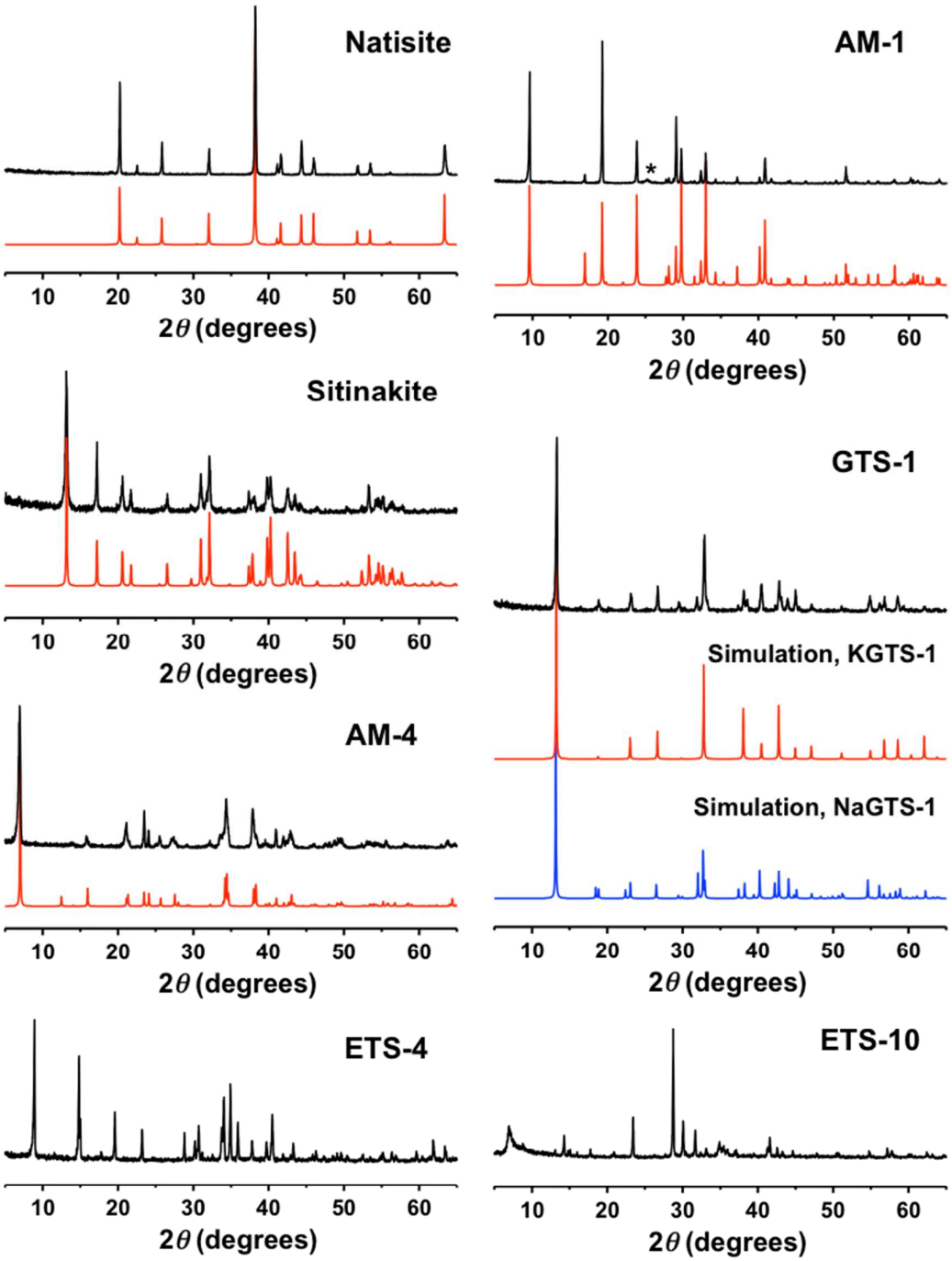

Figure S1. The powder XRD patterns of titanosilicates are shown above. The black trace is experimental data, the red trace are simulations based on reported crystal structures. The asterisk (*) denotes an impurity.

Table S1. $^{47/49}$Ti SSNMR acquisition parameters at 21.1 T.

Sample	Experiment	Pulse delay (s)	Number of scans [a]
Natisite	WURST-CPMG	1	2048
	WURST echo	0.5	65536[b]
	Quadrupolar echo	0.5	49152
AM-1	WURST-CPMG	0.5	24588 (3 × 8196)
	WURST echo	0.5	98304[b]
AM-4	WURST-CPMG	0.5	24588 (3 × 8196)
	Quadrupolar echo	0.5	49152
Sitinakite	Quadrupolar echo	1	49152
GTS-1	Quadrupolar echo	0.5	123904
	WURST-CPMG	0.5	24588 (3 × 8196)
ETS-10	Quadrupolar echo	1	49152
ETS-4	Quadrupolar echo	0.5	118784

[a] The value given is the total number of scans. In cases where the powder pattern is constructed from several "pieces" or subspectra, this value denotes the total number of scans performed on the entire powder pattern, not the number of scans of each subspectrum (except for WURST-echo, see footnote [b]). The WURST-CPMG spectra of AM-1, AM-4, and GTS-1 were assembled from three individual subspectra, all other spectra did not require piecewise addition. All subspectra were acquired for an equal number of scans (8196). [b] The overall echo spectrum was co-added from two individual experiments that used opposing WURST frequency sweep directions (Natisite: 2 × 32768 scans, AM-1: 2 × 49152 scans).

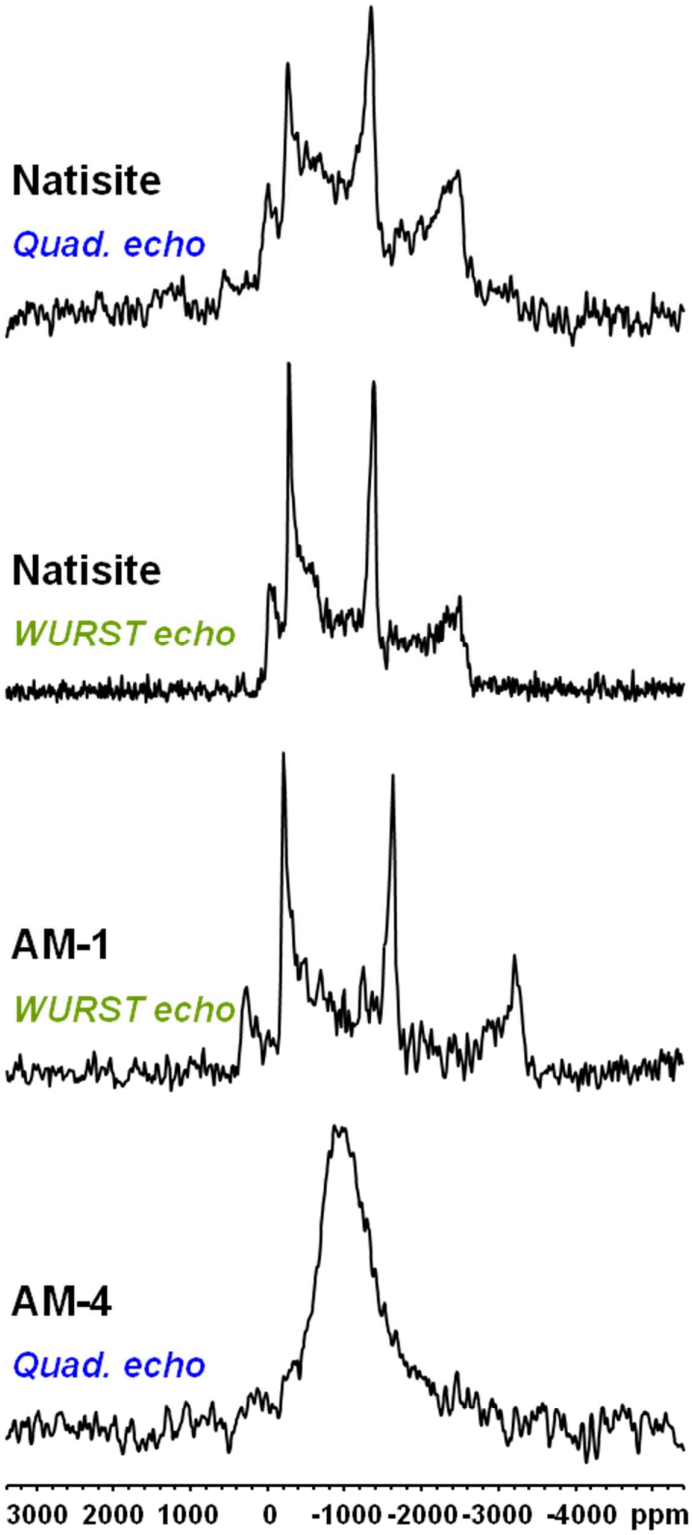

Figure S2. $^{47/49}$Ti SSNMR echo spectra of several titanosilicates are shown above. The colored text indicates the pulse sequence used to obtain the spectra, where "Quad. echo" refers to the quadrupolar echo pulse sequence.

Section S1. ^{29}Si and ^{23}Na SSNMR experimental parameters

^{29}Si MAS SSNMR experiments were performed on a Varian Infinity Plus 400 wide-bore spectrometer at a magnetic field of 9.4 T (ν_0(^{29}Si) = 79.36 MHz) using a 7.5 mm HXY MAS probe operating at spinning frequency of 5 kHz. All spectra were acquired using a Bloch-decay (i.e., one-pulse) sequence which employed 40 kHz continuous-wave ^{1}H decoupling. The number of scans acquired for each compound range from 84 to 128. A pulse length of 3 μs (corresponding to a 45° ^{29}Si pulse) and a recycle delay of 60 s were used. The ^{29}Si chemical shift was referenced using the downfield peak of tris(trimethylsilyl)silane (TTMSS), which is located at –9.8 ppm relative to the peak in tetramethylsilane (TMS) at 0.0 ppm.

^{23}Na SSNMR experimental conditions are shown in Table S2. Rotor-synchronized ^{23}Na 3QMAS spectra were acquired at a spinning frequency of 20 kHz using the standard Z-filter MQMAS sequence.[1] The excitation, conversion and selection pulse widths of ^{23}Na were optimized and set as 2.86, 1.03 and 10.00 μs, respectively. FID signals were Fourier-transformed and sheared using the Varian Spinsight software to obtain the separate F1 and F2 dimensions. ^{23}Na spin-lattice relaxation times (T_1) were measured using the inversion-recovery 180° - τ - 90° sequence (Table S2) to ensure accurate relative intensities of Na^+ sites. The intensity-τ plots were fitted by a three-component equation using the Spinsight software.

Table S2. ^{23}Na SSNMR acquisition parameters at 9.4 T.

Sample	Experiment	Pulse delay (s)	T_1 (s)	Number of scans
Natisite	MAS	2	0.75	512
	3QMAS	2		19968 (312 × 64)
AM-1	MAS	2	0.35	512
AM-4	MAS	2	0.16	1024
	3QMAS	2		19968 (312 × 64)
GTS-1	MAS	2, 0.2	0.0012	512
	3QMAS	2		19968 (312 × 64)
ETS-10	MAS	0.5	0.0074	1024
	3QMAS	0.5		76800 (600 × 128)
ETS-4	MAS	1	0.0013	1024
	3QMAS	0.5		19968 (312 × 64)

Section S2. ^{23}Na MAS and 3QMAS spectra

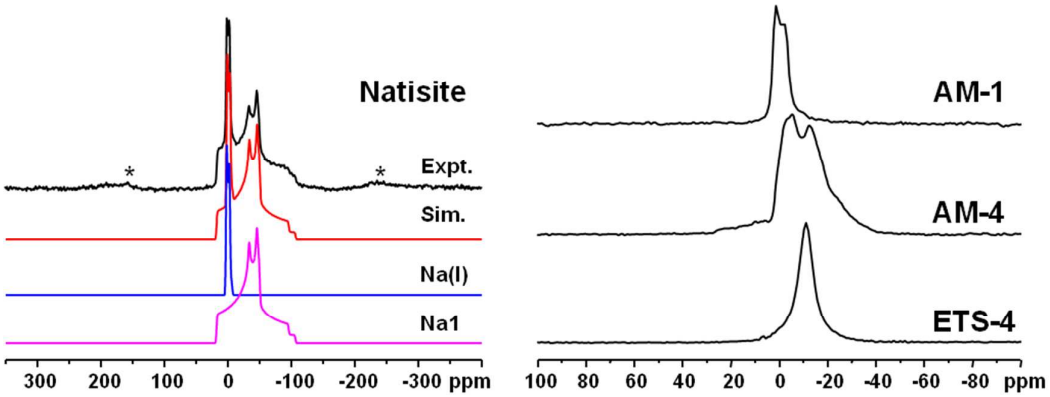

Figure S3. ^{23}Na MAS SSNMR spectra at 9.4 T. Spinning sidebands are denoted by *. Note the differences in chemical shift scales between natisite and the other compounds; the natisite powder pattern is significantly broader.

To the best of our knowledge, this is the first report of ^{23}Na SSNMR of natisite, and a detailed discussion of those experimental results is provided in the main text. The ^{23}Na MAS spectra of AM-1, AM-4 and ETS-4 closely resemble those described in previous reports.[2-5] ^{23}Na 3QMAS spectra are depicted in Figure S3. The ^{23}Na 3QMAS spectra of AM-4, sitinakite and ETS-10 appear similar to prior accounts.[2-3, 6-8]

The two Na sites observed in the MAS spectrum of natisite are clearly resolved in the 2D 3QMAS spectrum. Two Na sites were also resolved in the 3QMAS spectrum of ETS-4. Unfortunately, it was not possible to fully differentiate the two Na sites of GTS-1 *via* 3QMAS experiments.

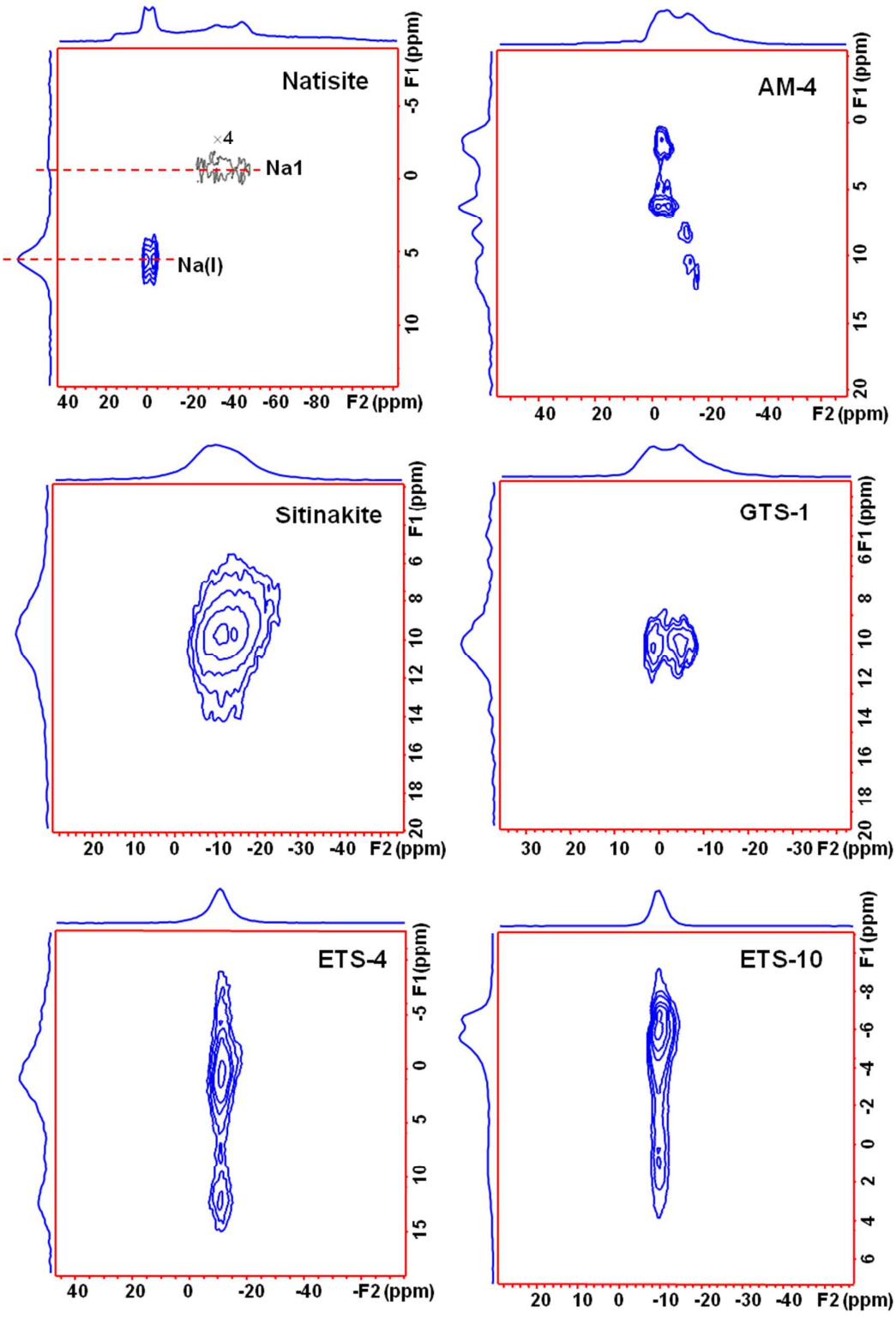

Figure S4. ^{23}Na 3QMAS spectra at 9.4 T.

Section S3. ^{29}Si MAS SSNMR spectra

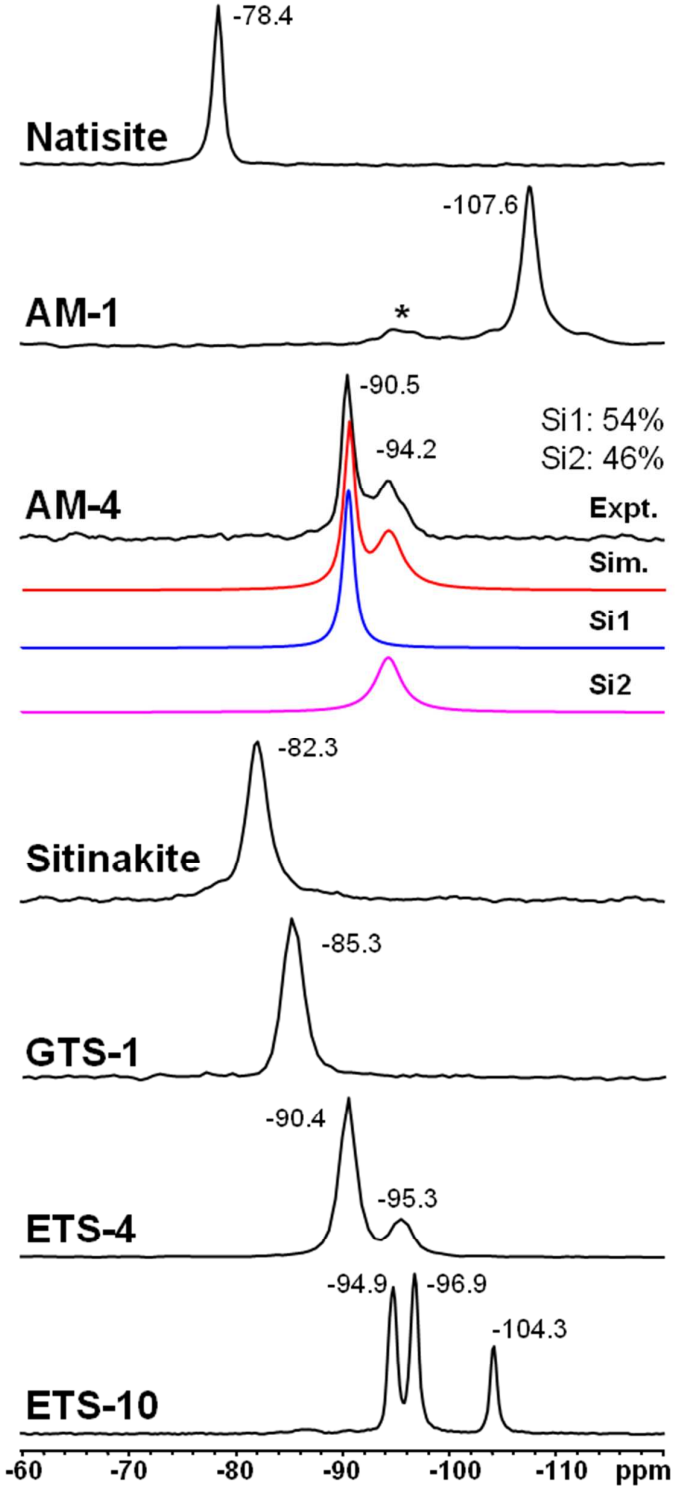

Figure S5. ^{29}Si MAS SSNMR spectra at 9.4 T. *: impurity.

The ^{29}Si MAS spectra of our titanosilicate samples look quite similar to those in the literature,[2-5, 9-10] except for natisite and AM-4; these two spectra are discussed in the main text. The spectrum of AM-1 displays a slight Si impurity at ca. -95 ppm whose origins are unknown.

The two polymorphs of ETS-10

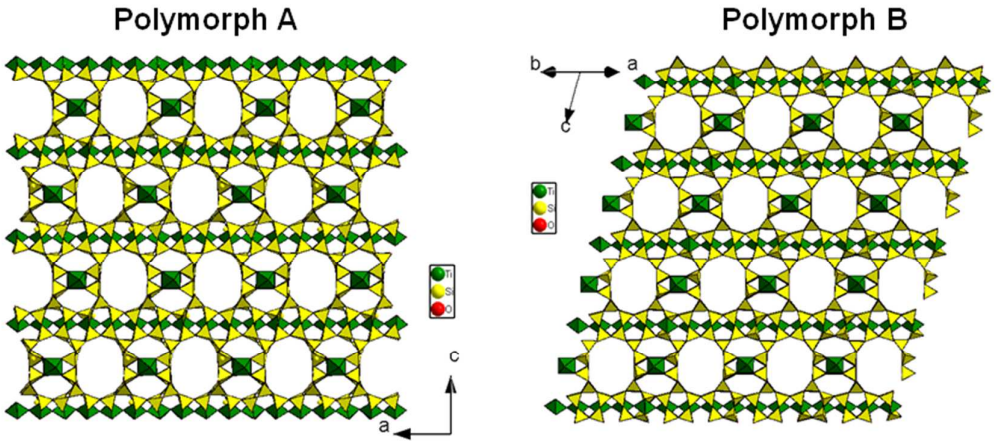

Figure S6. The structures of two polymorphs of ETS-10. It is possible to describe the structure of ETS-10 in terms of an intergrowth of two ordered polymorphs with tetragonal (polymorph A) and monoclinic (polymorph B) symmetry. The combined presence of both polymorphs leads to intrinsic disorder and structural faulting within ETS-10.

Section S4. $^{47/49}$Ti and ^{23}Na SSNMR experiments on ETS-4

The framework of ETS-4 ($Na_8(Ti_5H_2Si_{12}O_{39})(H_2O)_{8.45}$, Si/Ti ≈ 2.1 from EDS) contains distorted octahedral TiO_6 chains, isolated square-pyramidal TiO_5 units, and tetrahedral SiO_4 (Figure S7).[11] The TiO_6 octahedra contain the crystallographic Ti1 site and connect to each other by corner-sharing, forming –O–Ti–O–Ti–O– chains along the *b* axis in a distinct fashion that contrasts with the edge-sharing brookite-type chains in AM-4. The individual TiO_6 octahedra are significantly distorted, giving rise to O–Ti–O bond angles that range from 63 ° to 116 °, far from the idealized 90 °. The crystallographic Ti2 site is located in TiO_5 square-pyramids with four basal oxygen atoms shared with four neighboring symmetry-related SiO_4 units. Within ETS-4, interactions between neighboring TiO_5 pyramids are mediated *via* water molecules incorporated into the molecular structure. The anionic framework charges are balanced by extra-framework Na^+ cations. ETS-4 exhibits an intrinsic disorder of the framework, originating from three sources: i) the 12-rings are only partially occupied by TiO_5 units (occupancy: 0.25); ii) the orientation of TiO_5 units with respect to the rest of the framework is random; and iii) water molecules mediating the interactions between neighboring TiO_5 units are also disordered, although this disorder does not cause the termination of the TiO_6 chain.

The acquisition of natural abundance $^{47/49}$Ti static echo spectrum of ETS-4 was very challenging, even at 21.1 T. After 16 h of experimental acquisition, the spectrum (Figure S7(b)) obtained consists of a weak and very broad profile from ca. 900 to –2600 ppm. Simulation and interpretation of this $^{47/49}$Ti spectrum is quite challenging

due to the poor S/N, uninformative lineshape, and Ti disorder within this system. Although a signal is obtained, it cannot be unambiguously attributed to one, two, or more resonances; correspondingly, even crude $^{47/49}$Ti EFG tensor parameters are unavailable. ^{23}Na MAS and 3QMAS experiments on ETS-4 were successful and two ^{23}Na sites were resolved, but these experiments did not provide additional insight into this compound (Figures S3 and S4, Table A2).

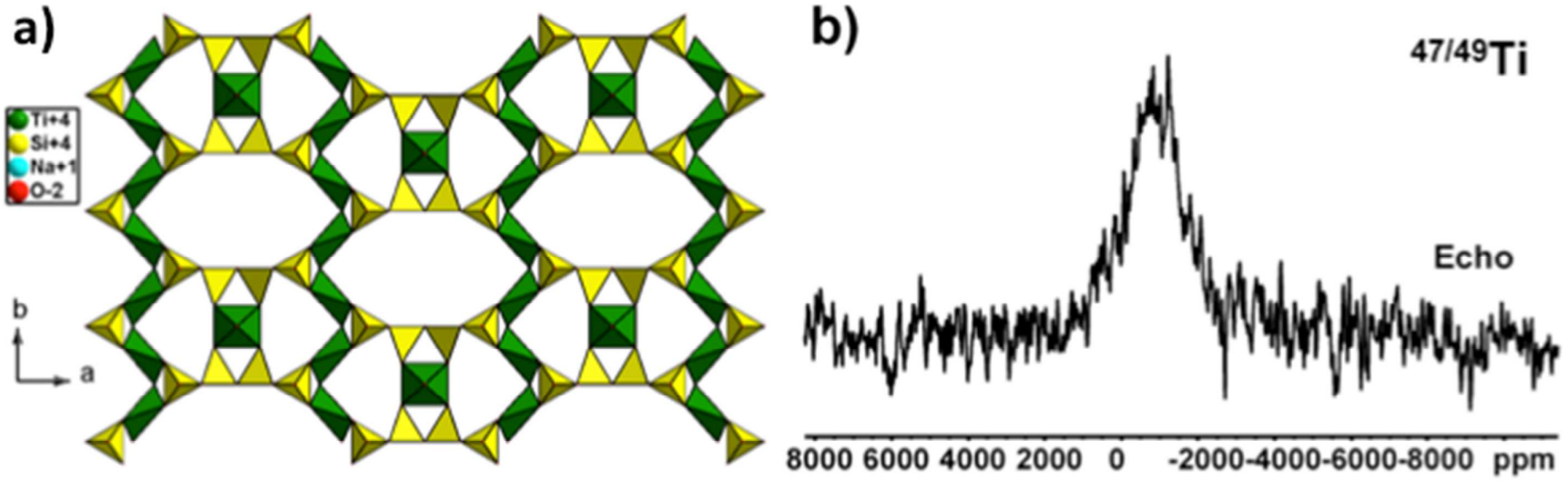

Figure S7. (a) The structure of ETS-4 (The water molecules and Na^+ cations are omitted for clarity). (b) Experimental (echo) natural abundance $^{47/49}$Ti static spectra of ETS-4 at 21.1 T.

Appendix A: Plane-wave DFT calculations of ^{23}Na, ^{29}Si, and $^{47/49}$Ti NMR tensor parameters

We have calculated ^{29}Si, ^{23}Na and ^{49}Ti NMR tensor parameters for five titanosilicates: natisite, AM-1, AM-4, sitinakite and NaGTS-1. The experimental and calculated NMR parameters of ^{29}Si, ^{23}Na and ^{49}Ti are shown in Tables A1, A2, and A3, respectively, while correlations of experimental and calculated NMR parameters are depicted in Figures A1 and A2.

As Figure A1 illustrates, a linear relationship was observed between the calculated isotropic chemical shielding of ^{29}Si (σ_{iso}(^{29}Si)) and the experimental isotropic chemical shift (δ_{iso}(^{29}Si)), with a line of best fit that indicates δ_{iso}(^{29}Si) = -0.673σ_{iso}(^{29}Si) + 186.9 (in units of ppm). These calculations were used to help assign the two ^{29}Si SSNMR resonances of AM-4. The two crystallographic Si sites of AM-4 are difficult to assign using only qualitative arguments involving coordination, because although Si1 has 3 neighboring Ti^{4+} and Si2 has only 1, Si1 has 2 neighboring Na^{+} centres versus the 6 Na^{+} proximate to Si2. Plane-wave DFT results suggest that the less shielded resonance at -90.5 ppm belongs to Si1 while the more shielded resonance at -94.2 ppm is assigned to Si2.

Based on the four titanosilicate samples with ordered Na sites (natisite, AM-1, AM-4 and NaGTS-1), reasonably linear relationships between calculated and experimental ^{23}Na C_Q and η_Q exist (Figure A1 (b),(c)). The only major discrepancy between calculated and experimental C_Q(^{23}Na) values is for sitinakite. There is no correlation between experimentally-measured δ_{iso} values and calculated σ_{iso} values

(Figure A2). It seems that plane-wave DFT calculations are valuable for the interpretation of ^{23}Na SSNMR spectra for these types of systems, but only as it pertains to ^{23}Na EFG parameters.

To relate chemical shieldings to shifts, as well as assess the reliability of calculations, ^{49}Ti NMR parameters were calculated for $MTiO_3$ (M = Mg, Ca, Sr, Ba) and three TiO_2 polymorphs in addition to experimental compounds. Calculated ^{49}Ti EFG tensor parameters (C_Q, η_Q) generally agree well with experimental values (Figure A1 (d), (e)). Calculations predict that only the span (Ω) values of natisite and AM-1 will be large enough to make a quantifiable contribution to $^{47/49}$Ti SSNMR spectra, in good agreement with experimental observations. The link between δ_{iso} and calculated σ_{iso} values is relatively weak, but good agreement still exists in most experimental cases, owing to the inclusion of the additional model Ti compounds in calculations and the correlation plot.

Calculations of C_Q(^{49}Ti) can be used to interpret the $^{47/49}$Ti SSNMR spectrum of GTS-1 pictured in Figure 5(b) of the main text. Recalling that our GTS-1 sample was a mixture of KGTS-1 and NaGTS-1, we have assigned the resonance observable in the $^{47/49}$Ti SSNMR spectrum of our GTS-1 sample to the crystallographic Ti2 site of NaGTS-1. The degree of distortion associated with the Ti1 site (Ti—O: 1.828-2.107 Å) of NaGTS-1 is significantly larger than that of Ti2 within NaGTS-1 (Ti—O: 1.983-2.100 Å), yielding a $^{47/49}$Ti SSNMR pattern that is of weak intensity and is too broad to be measured, even using an ultra-highfield of 21.1 T. Plane-wave DFT calculations support this conclusion; the calculated C_Q(Ti1) value of 39.25 MHz is

more than three times larger than the calculated C_Q(Ti2) value of 10.13 MHz. But what of KGTS-1, which normally exhibits an ordered crystal structure and thus should be observed in the $^{47/49}$Ti SSNMR spectrum? The ^{39}K SSNMR spectrum of KGTS-1 shows that a significant fraction of the K^+ sites in GTS-1 are disordered (Figure 6(b)), injecting a large degree of uncertainty into plane-wave DFT calculations. Unfortunately, attempts to calculate the $C_Q(^{49}Ti)$ of KGTS-1 fail without the reduction of crystal symmetry. We can instead qualitatively estimate the $C_Q(^{49}Ti)$ of KGTS-1 by comparing the degree of distortion of TiO_6 units. The Ti—O bond length distribution of the single Ti site of KGTS-1 (1.851-2.048 Å) is relatively large and comparable to that of the Ti1 site of NaGTS-1. It follows that, much like the Ti1 site of NaGTS-1, the $C_Q(^{49}Ti)$ of the Ti site in KGTS-1 most likely results in a $^{47/49}$Ti SSNMR powder pattern that is simply too broad and of too low S/N to be detected at 21.1 T.

Table A1. Experimental and calculated ^{29}Si NMR parameters.

			δ_{iso} (ppm)		σ_{iso} (ppm)
Sample	**Si Site**	**Si Environment**	**Experimental**	**Calculated[a]**	**Calculated**
Natisite	Si1	Si(4Ti)	-78.4	-83.7	402.15
AM-1	Si1	Si(1Ti)	-107.6	-105.2	434.07
AM-4[b]	Si1	Si(3Ti)	-90.5	-92.4	414.95
	Si2	Si(1Ti)	-94.2	-94.8	418.57
Sitinakite	Si1	Si(4Ti)	-82.3	-77.7	393.23
NaGTS-1	Si1	Si(4Ti)	-85.3	-84.2	402.82
ETS-4	Si(I)	Si(3Ti)	-90.4	-	-
	Si(II)	Si(1Ti)	-95.3	-	-
ETS-10	Si(I)	Si(1Ti)	-94.9	-	-
	Si(II)	Si(1Ti)	-96.9	-	-
	Si(III)	Si(0Ti)	-104.3	-	-

[a] Calculated σ_{iso} values were converted to δ_{iso} by using the relationship δ_{iso} = -0.673σ_{iso} +186.9, the line of best fit corresponding to the graph in Figure A1(a). [b] This structure was not geometry optimized prior to calculation of NMR tensor parameters, unlike all others.

Table A2. Experimental and calculated ^{23}Na NMR parameters.

Sample	Na site	Na coordination	$\|C_Q\|$ (MHz)		η_Q		δ_{iso} (ppm)		σ_{iso} (ppm)
			Experimental	Calculated	Experimental	Calculated	Experimental	Calculated[a]	Calculated
Natisite	Na1	6	4.5(1)	4.28	0.8(1)	0.81	18.6(2)	4.5	544.28
	Na(I)		1.4(1)	-	0.0(1)	-	3.0(6)	-	-
AM-1	Na1	6	1.4(1)	1.75	0.2(1)	0.22	4.0(6)	4.0	434.07
AM-4	Na1	6	2.1(1)	2.21	1.0(1)	0.80	0.9(10)	4.6	559.96
	Na2	6	1.7(1)	1.47	0.3(1)	0.31	-3.0(10)	4.6	557.40
	Na3	4	2.5(1)	3.90	0.9(1)	0.88	0.3(10)	4.4	523.36
	Na(I)		1.3(1)	-	0.0(1)	-	1.1(10)	-	-
Sitinakite	Na(I)	6	1.9(1)	6.22	0.5(1)	0.69	0.4(10)	4.6	561.20
	Na(II)	6	1.9 ± 0.9	4.98	0.9 ± 0.1	0.53	5.7	4.8	602.54
NaGTS-1	Na1	4	1.8(1)	1.92	0.1(1)	0.00	6.0(10)	4.8	596.38
	Na2	6	2.2(1)	3.50	1.0(1)	0.63	8.3(10)	4.6	551.98
ETS-4	Na1		1.8(1)	-	0.8(1)	-	-1.7(5)	-	-
	Na2		1.6(1)	-	0.8(1)	-	-3.4(5)	-	-
ETS-10	Na(I)		1.0(1)	-	0.4(2)	-	-7.4(10)	-	-
	Na(II)		1.1(1)	-	0.5(2)	-	-6.2(10)	-	-
	Na(III)		1.2(1)	-	0.5(2)	-	-6.1(10)	-	-
	Na(IV)		1.2(1)	-	0.6(2)	-	-5.9(10)	-	-

[a] Calculated σ_{iso} values were converted to δ_{iso} by using the relationship $\delta_{iso} = 0.0048\sigma_{iso} + 1.9277$, the line of best fit corresponding to the graph in Figure A2. It should be noted that there is no measurable correlation in that graph, hence, calculated δ_{iso} values match experimental δ_{iso} values poorly in most cases.

Table A3. Experimental and calculated ^{49}Ti NMR parameters.[a]

Sample	Ti site	Ti coordination	$\lvert C_Q \rvert$ (MHz)		η_Q		δ_{iso} (ppm)		σ_{iso} (ppm)	Ω (ppm)		κ	
			Expt.	Calc.	Expt.	Calc.	Expt.	Calc.	Calc.	Expt.	Calc.	Expt.	Calc.
Natisite	1	5	10.7(1)	9.88	0.05(5)	0.00	-740(30)	-769.5	-297.33	500(30)	644.94	1.0(1)	1.00
AM-1	1	5	13.4(1)	17.05	0.05(5)	0.00	-783(30)	-874.1	-180.30	500(30)	705.39	1.0(1)	1.00
AM-4	1	6	8.2(2)	11.13	1.0(1)	0.92	-850(30)	-916.7	-132.71	-	127.35	-	0.55
Sitinakite	1	6	13 ± 11	8.70	0.85 ± 0.15	0.45	-950	-922.8	-125.80	-	97.83	-	0.68
NaGTS-1	1	6	-	39.25	-	0.00	-	-951.0	-94.26	-	52.44	-	1.00
	2	6	11.0(5)	10.13	0.4(2)	0.52	-900(40)	-921.1	-127.69	-	129.56	-	0.20
ETS-10	1	6	16.5(2)	-	0.85(10)	-	-1100(50)	-	-	-	-	-	-
Rutile	1	6	13.9	10.45	0.19	0.43	-843	-899.8	-151.58	-	122.92	-	0.03
Anatase	1	6	4.7	4.85	0	0.00	-1038	-949.0	-96.52	-	141.38	-	1.00
Brookite	1	6	6.04	7.20	0.55	0.39	-943	-949.8	-95.69	-	173.96	-	-0.66
$MgTiO_3$	1	6	15.52(5)	13.86	0.00(5)	0.00	-993(10)	-862.2	-193.67	-	176.70	-	0.00
$CaTiO_3$	1	6	2.75(1)	3.02	0.70(6)	0.95	-853.5(10)	-857.3	-199.16	-	42.04	-	-0.81
$SrTiO_3$	1	6	≈ 0	≈ 0	N/A	N/A	-843	-835.0	-224.09	-	N/A	-	N/A
$BaTiO_3$	1	6	3.42(5)	2.39	0.00(5)	0.00	-731(1)	-709.8	-364.12	22.5(1)	2.60	1	1.00

[a] All experimental data for rutile,[12] anatase,[12-14] and brookite TiO_2,[15] as well as MTiO3 (M = Mg,[16] Ca,[12, 16] Sr,[17] Ba[16]) was taken from the literature.[18] Calculations on these compounds were performed using the crystal structures of rutile,[19] anatase,[20] and brookite[21] TiO_2, as well as MTiO3 (M = Mg,[22] Ca,[23] Sr,[24] Ba[25]) after geometry optimization. [b] Chemical shifts (δ_{iso}) were calculated by using the formula $\delta_{iso} = -0.894\sigma_{iso} - 1035.3$, which is the line of best fit on a graph of experimental δ_{iso} vs. calculated σ_{iso} (Figure A1(f)).

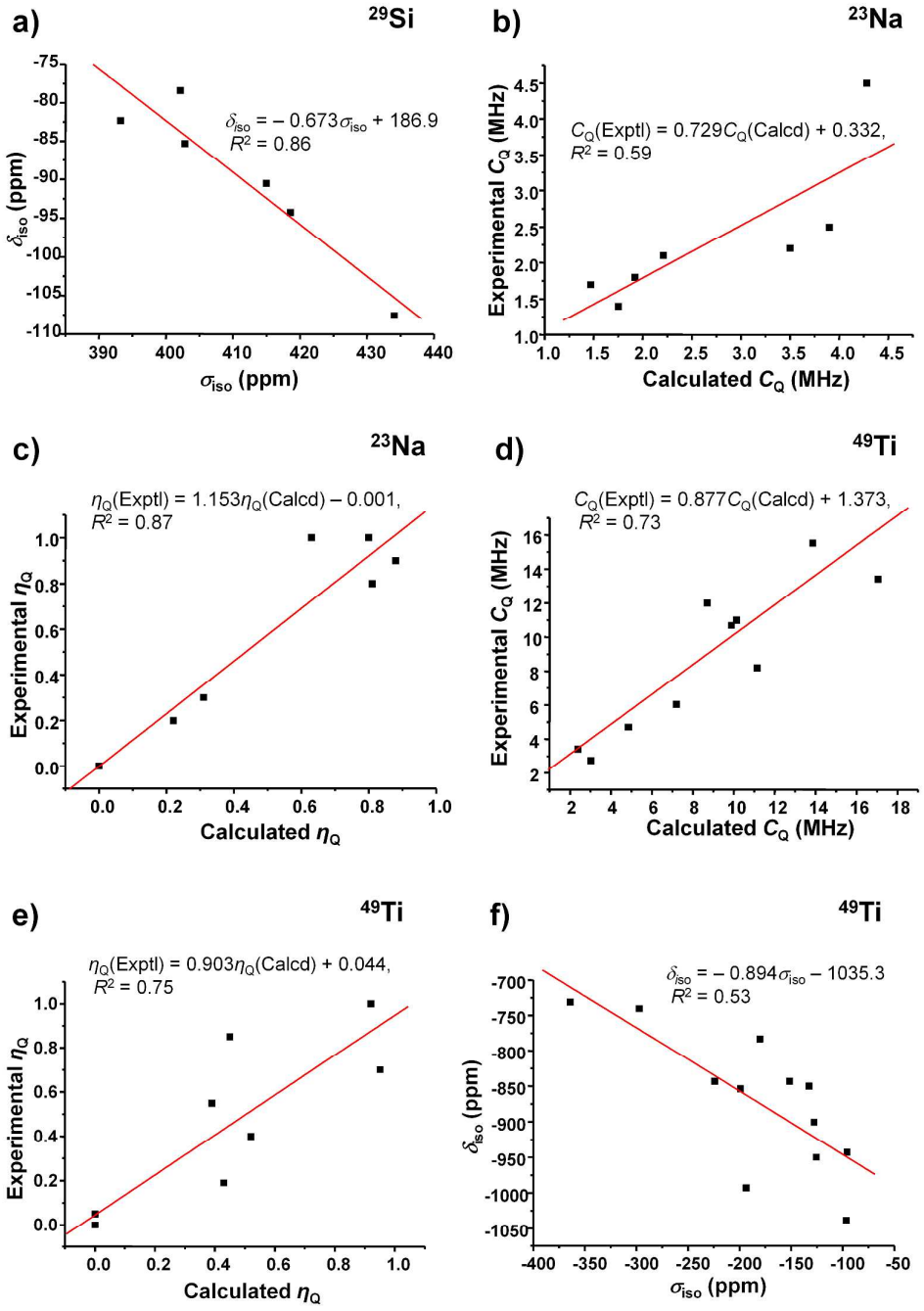

Figure A1. Correlation between the measured ^{29}Si δ_{iso} (a), ^{23}Na C_Q (b) and η_Q (c), ^{49}Ti C_Q (d), η_Q (e) and δ_{iso} (f) with the calculated values.

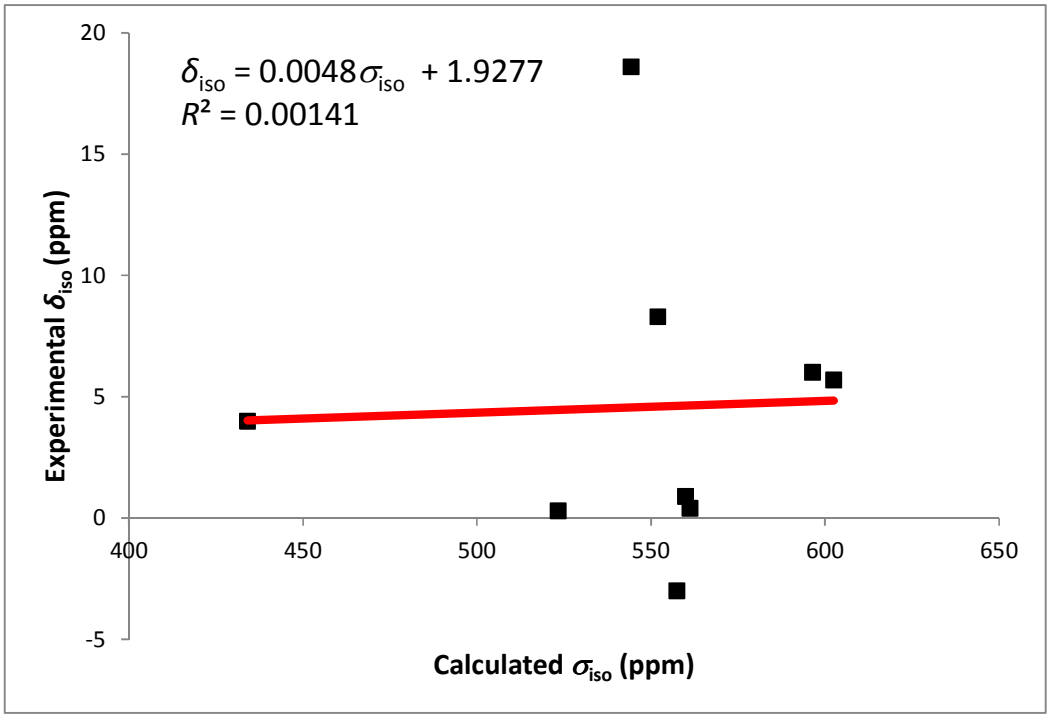

Figure A2. A plot of experimental ^{23}Na chemical shifts versus calculated ^{23}Na chemical shieldings. There is no clear correlation, resulting in calculated chemical shifts that stray significantly from experimental values (Table A2).

References

1. Amoureux, J. P.; Fernandez, C.; Steuernageel, S. Z Filtering in MQMAS NMR. *J. Magn. Reson., Ser. A.* **1996**, *123*, 116-118.

2. Lin, Z.; Rocha, J.; Brandao, P.; Ferreira, A.; Esculcas, A. P.; Pedrosa de Jesus, J. D.; Philippou, A.; Anderson, M. W. Synthesis and Structural Characterization of Microporous Umbite, Penkvilksite, and Other Titanosilicates. *J. Phys. Chem. B* **1997**, *101*, 7114-7120.

3. Cherry, B. R.; Nyman, M.; Alam, T. M. Investigation of Cation Environment and Framework Changes in Silicotitanate Exchange Materials Using Solid-State ^{23}Na, ^{29}Si, and ^{133}Cs MAS NMR. *J. Solid State Chem.* **2004**, *177*, 2079-2093.

4. Thorogood, G. J.; Kennedy, B. J.; Griffith, C. S.; Elcombe, M. M.; Avdeev, M.; Hanna, J. V.; Thorogood, S. K.; Luca, V. Structure and Phase Transformations in the Titanosilicate, Sitinakite. The Importance of Water. *Chem. Mater.* **2010**, *22*, 4222-4231.

5. Kostov-Kytin, V.; Nikolova, R.; Nakayama, N.; Simova, S.; Tzvetkova, P. New Data on Crystal Chemistry of Nano-Sized Microporous Titanosilicates with Pharmacosiderite Structure. *C. R. Acad. Bulg. Sci.* **2011**, *64*, 683-692.

6. Ganapathy, S.; Das, T. K.; Vetrivel, R.; Ray, S.; Sen, T.; Sivasanker, S.; Delevoye, L.; Fernandez, C.; Amoureux, J. P. Anisotropic Chemical Shielding, M-Site Ordering, and Characterization of Extraframework Cations in ETS-10 Studied through MAS/MQ-MAS NMR and Molecular Modeling Techniques. *J. Am. Chem. Soc.* **1998**, *120*, 4752-4762.

7. Anderson, M. W.; Agger, J. R.; Luigi, D.-P.; Baggaley, A. K.; Rocha, J. Cation Sites in ETS-10: ^{23}Na 3Q MAS NMR and Lattice Energy Minimization Calculations. *Phys. Chem. Chem. Phys.* **1999**, *1*, 2287-2292.

8. Southon, P. D.; Howe, R. F. Spectroscopic Studies of Disorder in the Microporous Titanosilicate ETS-10. *Chem. Mater.* **2002**, *14*, 4209-4218.

9. Anderson, M. W.; Terasaki, O.; Ohsuna, T.; Philippou, A.; Mackay, S. P.; Ferreira, A.; Rocha, J.; Lidin, S. Structure of the Microporous Titanosilicate ETS-10. *Nature* **1994**, *367*, 347-351.

10. Balmer, M. L.; Bunker, B. C.; Wang, L. Q.; Peden, C. H. F.; Su, Y. Solid-State ^{29}Si MAS NMR Study of Titanosilicates. *J. Phys. Chem. B* **1997**, *101*, 9170-9179.

11. Cruciani, G.; De Luca, P.; Nastro, A.; Pattison, P. Rietveld Refinement of the Zorite Structure of ETS-4 Molecular Sieves. *Micropor. Mesopor. Mat.* **1998**, *21*, 143-153.

12. Bastow, T. J.; Gibson, M. A.; Forwood, C. T. ^{47}Ti, ^{49}Ti NMR: Hyperfine Interactions in Oxides and Metals. *Solid State Nucl. Magn. Reson.* **1998**, *12*, 201-209.

13. Kanert, O.; Kolem, H. The Unusual Temperature-Dependence of the Electric-Field Gradient at Titanium Sites in Rutile (TiO_2). *Journal of Physics C-Solid State Physics* **1988**, *21*, 3909-3916.

14. Labouriau, A.; Earl, W. L. Titanium Solid-State NMR in Anatase, Brookite and Rutile. *Chem. Phys. Lett.* **1997**, *270*, 278-284.

15. Bastow, T. J.; Doran, G.; Whitfield, H. J. Electron Diffraction and ^{47}Ti, ^{49}T and ^{17}O NMR Studies of Natural and Synthetic Brookite. *Chem. Mater.* **2000**, *12*, 436-439.

16. Padro, D.; Howes, A. P.; Smith, M. E.; Dupree, R. Determination of Titanium Nmr Parameters of $ATiO_3$ Compounds: Correlations with Structural Distortion. *Solid State Nucl. Magn. Reson.* **2000**, *15*, 231-236.

17. Dec, S. F.; Davis, M. F.; Maciel, G. E.; Bronnimann, C. E.; Fitzgerald, J. J.; Han, S. S. Solid-State Multinuclear NMR Studies of Ferroelectric, Piezoelectric, and Related Materials. *Inorg. Chem.* **1993**, *32*, 955-959.

18. Mackenzie, K. J. D.; Smith, M. E., *Multinuclear Solid-State Nuclear Magnetic Resonance of Inorganic Materials*. Pergamon Press: Oxford, UK, 2002.

19. Meagher, E. P.; Lager, G. A. Polyhedral Thermal Expansion in the TiO_2 Polymorphs: Refinement of the Crystal Structures of Rutile and Brookite at High Temperature. *Can. Mineral.* **1979**, *17*, 77-85.

20. Wyckoff, R. W. G., *Crystal Structures*. Interscience Publishers: New York, 1963.

21. Pauling, L.; Sturdivant, J. H. The Crystal Structure of Brookite. *Z. Kristallogr.* **1928**, *68*, 239-256.

22. Wechsler, B. A.; Vondreele, R. B. Structure Refinements of Mg_2TiO_4, $MgTiO_3$ and $MgTi_2O_5$ by Time-of-Flight Neutron Powder Diffraction. *Acta Crystallogr. Sect. B: Struct. Sci.* **1989**, *45*, 542-549.

23. Liu, X.; Liebermann, R. C. X-Ray-Powder Diffraction Study of $CaTiO_3$ Perovskite at High-Temperatures. *Phys. Chem. Miner.* **1993**, *20*, 171-175.

24. Mitchell, R. H.; Chakhmouradian, A. R.; Woodward, P. M. Crystal Chemistry of Perovskite-Type Compounds in the Tausonite-Loparite Series, $(Sr_{1-2x}Na_xLa_x)TiO_3$. *Phys. Chem. Miner.* **2000**, *27*, 583-589.

25. Buttner, R. H.; Maslen, E. N. Structural Parameters and Electron Difference Density in $BaTiO_3$. *Acta Crystallogr. Sect. B: Struct. Sci.* **1992**, *48*, 764-769.